Mechanical behavior of a 16 T FCC dipole magnet during a quench

Junjie Zhao[1,2*], Antti Stenvall[1], Tiina Salmi[1], Yuanwen Gao[2], Clement Lorin[3]

1 Institute of Electromagnetics, Tampere University of Technology, PO Box 692, 33101 Tampere, Finland

2 Department of Mechanics and Engineering Science, College of Civil Engineering and Mechanics, Lanzhou University, Lanzhou, Gansu 730000, PR China

3 CEA Saclay, 91191 Gif-sur-Yvette, France

[*]Corresponding author: zhaojj15@lzu.edu.cn

Abstract

Future accelerator magnets are pushed to their limits in terms of magnetic field and also from the quench protection point of view. This forces the magnet designers to re-think the quench modelling. One issue that has not so far been largely explored is the mechanical behaviour of the superconducting coils during a quench. This can cause limitations to the design of high field accelerator magnets. This paper focuses on mechanical behavior in the event of a quench of a Nb_3Sn 16 T dipole magnet currently developed in the framework of the EuroCirCol project in view of the Future Circular Collider conceptual design study. The thermo-mechanical analysis is performed through finite element modeling. The analysis takes into account the Lorentz force and the thermal stress due to the non-uniform temperature distribution in the winding during a quench.

Index terms- accelerator magnet**,** quench, finite element analysis, Lorentz forces, thermal stress.

I. INTRODUCTION

The Future Circular Collider (FCC) is a collaboration, whose main purpose is to produce a conceptual design report of a 100 km particle accelerator for producing hadron collisions of up to 100 TeV center-of-mass energy [1]. EuroCirCol is an EU H2020 [2] funded project aiming to design a 16 T Nb_3Sn dipole that could be used as a FCC main bending magnet [3]. Various 16 T magnet designs for the Future Circular Collider have been studied so far [4]-[5]. EuroCirCol 16 T dipole magnet design study includes three magnet design options: a block coil [6], a cos-θ [7]-[8] and common coil [5]. The present analysis deals with the mechanical impact of a quench in the block design option. One of the challenges in the design of such magnets is the high stored energy, which requires high reliability from the mechanical support structure and special attention from the magnet quench protection design.

Nb_3Sn is a strain sensitive material, whose critical current depends on strain and irreversible damage can occur at strain levels of 0.54% [9]. Due to the very low heat capacity at operation temperature of 1.8 K or 4.2 K, minor mechanical and thermal disturbances may cause superconductor to transfer to normal state and lead to a magnet quench. Due to high stored energy densities, after a quench the magnet temperature may rise up to 350 K, even in the cases with well-working quench protection system. Therefore, quantifying the thermal stress during a quench is important in order to analyze the risks for critical current degradation. Typically, the protection is triggered by the detection of a resistive voltage in the order of 100 mV across the transitioned zone. To avoid false quench detections, it is required that the voltage signal stays above the detection threshold for a given validation time (10 ms in the present LHC [10]). After the quench detection and validation, the magnet energy must be quickly damped to prevent damage due to local resistive heating. In high energy accelerator, external energy extraction is not a possible option because applying it fast enough would lead to too large terminal voltages. Typical maximum allowed terminal voltage is between 1 and 2 kV. Therefore, the stored energy in the magnet has to be absorbed by the magnet itself. This is obtained safely by using a quench protection system that quenches the whole coil and allows for a uniform energy dissipation. The protection system in large accelerators up to now has been based on resistive protection heaters placed on the coil surfaces. A novel method called Coupling Loss Induced Quench (CLIQ) [11], which has been explored recently, is based on discharging a capacitor into the coil. The coil will subsequently quench due to the induced inter-filament coupling losses. An indicator of the efficiency of quench protection systems is the time delay from its activation to the transition of the whole magnet.

During the first stages of the EuroCirCol magnet design, it was assumed that the protection system was able to spread the normal zone to the entire winding within 40 ms. In order to ensure the magnet protectability, it was set as a design criterion that the hotspot temperature must remain below 350 K [12]. In addition to the peak temperature, the internal voltages in the coil have been analysed in various cases. The aim of this paper is to add the analysis of stress during a quench into the study. After all, it is assumed that eventually mechanical failure will be the reason for degradation after a high temperature quench (either through epoxy break or the mechanical failure of Nb_3Sn material). The EuroCirCol 16 T magnet design options are particularly prone to high temperature differences during a quench because for economic reasons they are very compact and employ a graded design: Larger cable in high-field region to ensure enough superconductor, and smaller cable in low-field area. This results in unequal copper cross-section areas for the cables and consequently different heat generation. Because of the grading within a coil layer, the maximum temperature difference between two cables during a quench can be particularly large, around 100 K [12].

In this paper, we built a 2D finite element model of the magnet cross-section using the commercial simulation tool COMSOL [13], and computed the stress distribution during a magnet quench. The analysis takes into account the Lorentz forces and thermal stresses in addition to the stress resulting from the pre-load and cool down. The thermodynamic part of the quench modeling was done with Coodi [12] and used as an input for the COMSOL modeling.

II. MAGNET STRUCTURE

The present EuroCirCol block-type dipole design features a coil configuration with two double pancakes [6]. The magnet cross section, showing the iron yoke and the coils with two different Nb_3Sn cables is shown in Fig. 1 (a). The magnetic flux density distribution generated at nominal current is shown in Fig. 1 (b). Fig. 2 presents the magnet components in detail. Even though the final design can be a double-aperture configuration, we study here the so far designed single-aperture prototype design. This magnet utilizes for the pre-load so called bladder and key technology [14]-[15], which has been used in several high-field magnets developed recently [16]. The bladder is placed between the yoke and the inner iron pusher to create a clearance to insert the key (a set of stainless steel bars) and corresponding shims. Then, the bladder is deflated and removed, and the inserted keys provide the room temperature pre-stress. Then, during the cool down the thermal shrinkage of the external aluminum shell increases the pre-stress in the coil to fully compensate the stress due to Lorentz forces and to keep a good contact between the coil and the pole under operation. The magnet parameters are listed in Table I. The maximum horizontal and vertical Lorentz forces per aperture are 10500 kN/m and -5200 kN/m, respectively.

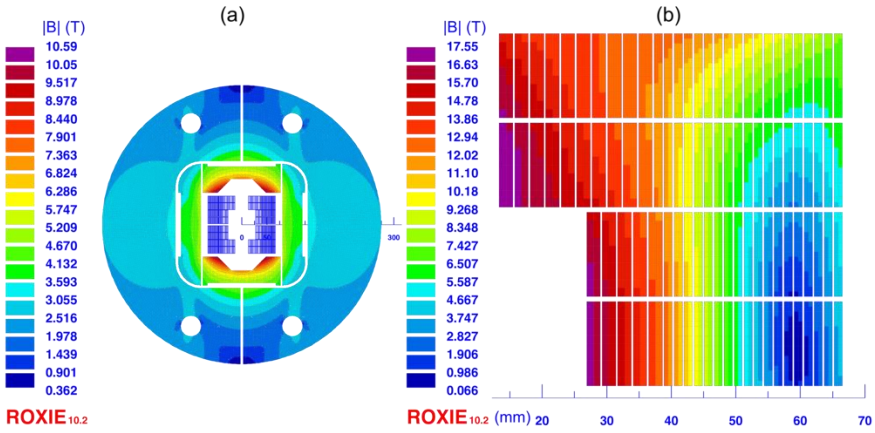

Fig. 1. (a) Magnet cross section within its iron yoke (b) Block coil cross-section made of two different Nb_3Sn cables and consisting of two double pancakes.

TABLE I. MAGNET PARAMETERS

Parameter	values
Nominal current	11470 A
Bore dipole field	16 T
Peak field in conductor	16.74 T
Operating temperature	1.9 K
Mid-plane shim thickness	1.75 mm
Loadline margin (1.9 K)	14.01%
Differential inductance at nominal current	18 mH/m
Stored energy at nominal current	1.2 MJ/m
Outer diameter of dipole	338 mm
Number of turns HF cable per coil	5+5+10+10=30
Number of turns LF cable per coil	18+18+19+19=74
Maximum Fx/Fy Lorentz force	10500 kN/m /-5200 kN/m

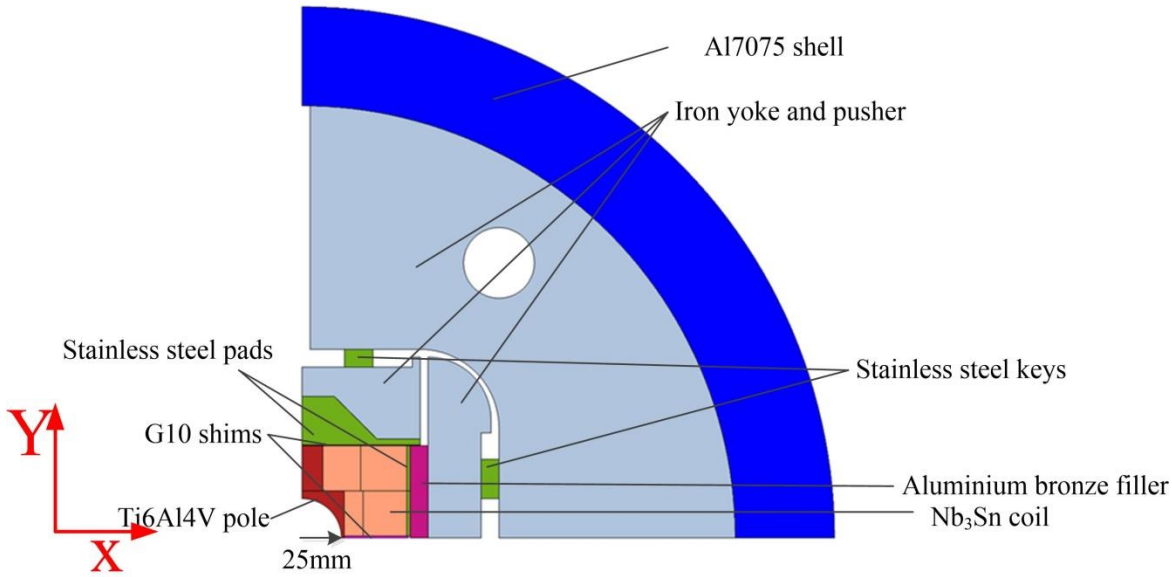

Fig. 2. One fourth of the magnet structure and the materials associated to each component.

III. COMPUTATION MODEL

An electromagnetic analysis and a preliminary mechanical study of the 16 T block-coil dipole magnet was presented in [17]. The present work extends the study to the mechanical behavior of the Nb_3Sn superconducting coil during a quench.

The 2D mechanical analysis includes the following steps: (i) Key insertion process. The key insertion process provides the pre-load at room temperature (RT). (ii) Cool down. The uniform temperature and the reference temperature are set to be 300 K at the beginning. Then the uniform temperature is decreased to 4.2 K homogeneously. The stress distribution changes due to the differences in the thermal expansion coefficients. (iii) Excitation. The Lorentz force is applied to the windings. The magnetostatic computation is done at 105% of the nominal current including the effect of iron magnetization. (iv) Quench process. During a quench, the Lorentz force is calculated at each simulation time for given current. The temperature distribution and the magnet current as a function of time are pre-computed with a tailor-made software called Coodi, and subsequently applied to the COMSOL mechanical model. The computation process of Coodi is detailed in [12]. The principal idea is to consider each turn adiabatic and isothermal. Then, the temperature of each turn is computed from the heat generation. When coupled to the magnet's circuit, the current decay can be modeled. Steps (i)-(iii) repeat the analysis presented in [17] and are considered here as the validation of the model.

In our 2D approximation, due to symmetry, it is sufficient to model one quarter of the magnet cross-section and plane stress model is assumed. The material properties for the magnet components are listed in Table II. These parameters are based on results from the tested High-Luminosity LHC prototype magnets developed by US LARP [18] and CERN [19]. In the finite element model, the Young modulus E and thermal expansion coefficient of the block coil is anisotropic (see TABLE II). For the key insertion process, the horizontal and vertical assembly interference between the key and the iron yoke are 750 μm and 50 μm, respectively. Two different types of contacts between the magnet components exist: those that are glued and those that can slide. Fig. 3 presents the mechanical structure with mesh and the different contact interface conditions. The friction coefficient of the sliding contact was 0.2. For the boundary conditions in the left side and the bottom side (at the symmetry axes), we set $\mathbf{n}\cdot\mathbf{u}=0$, where $\mathbf{u}$ is the displacement vector and $\mathbf{n}$ is the unit vector normal to the symmetry axes. The outer surface of the shell was free.

TABLE II. MATERIAL PROPERTIES

Component	Material	E (GPa) 293 K	E (GPa) 4.2 K	α (1/K)
Block Coil	Nb_3Sn	E_x=25,E_y=30, G_{xy}=21	E_x=27.5,E_y=33, G_{xy}=21	$\alpha_x=1.05\times10^{-5}$, $\alpha_y=1.15\times10^{-5}$
Magnetic pad and key	Steel 316LN	193	210	9.47×10^{-6}
Shell	Aluminum 7050	70	79	1.42×10^{-5}
Magnetic yoke and pusher	Iron	213	224	6.76×10^{-6}
Pole	Ti6Al4V	115	126.5	5.75×10^{-6}
Shim	G10	30	30	2.39×10^{-5}
Filler	Aluminum bronze	110	120	1.05×10^{-5}

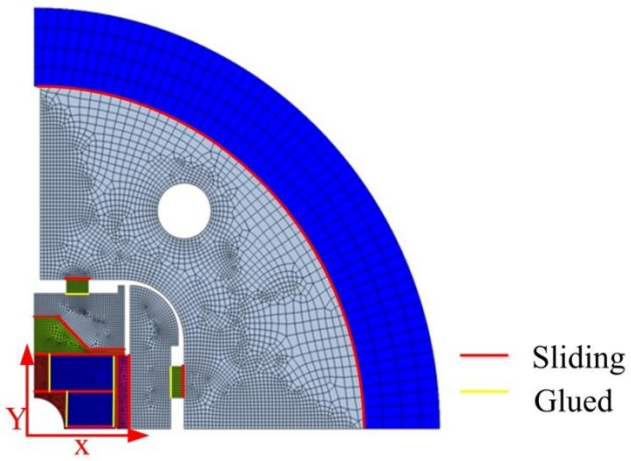

Fig. 3. One fourth of mechanical structure with mesh and contact interfaces.

IV. SIMULATED STRESS BEFORE QUENCH

To validate the analysis before the quench, we compared the results obtained with our model to those presented in [17] and computed with commercial software ANSYS. The maximum horizontal and von Mises stresses in the coils are reported in Table III. The von Mises stresses in the coils at different analysis steps are shown in Fig. 4. The horizontal stress distributions at different analysis steps are displayed in Fig. 5. The maximum von Mises stress in the coils is 126 MPa at warm and 200 MPa after cool down. The maximum von Mises stress of the coils decreased to 185 MPa when powered to 105% of the nominal operation current (12040 A). The maximum horizontal stress is

210 MPa after cool down and it decreases to 202 MPa for the operation at 105% of the nominal current. The peak von Mises stress is located at the corner of the center pole during pre-load and cool down step and it moves to the low field region of the coil after excitation.

The simulated von Mises stresses from the ANSYS and COMSOL models differ by less than 6% at the excitation. Reasons can be the different meshes, different non-linear solvers, or the way to apply the Lorentz force. However, we assume that this analysis validates our model and allows us to do predictions for the mechanical behaviors during the quench.

TABLE III. COMPARISON OF SIMULATED STRESS IN COILS AT ALL MODELLINGS STEPS

	Horizontal-stress (MPa)		von Mises stress (MPa)	
	COMSOL	ANSYS	COMSOL	ANSYS
Key insertion	-141	-135	126	121
Cool-down	-210	-216	200	196
Excitation @ 105% of the nominal current	-202	-195	185	176

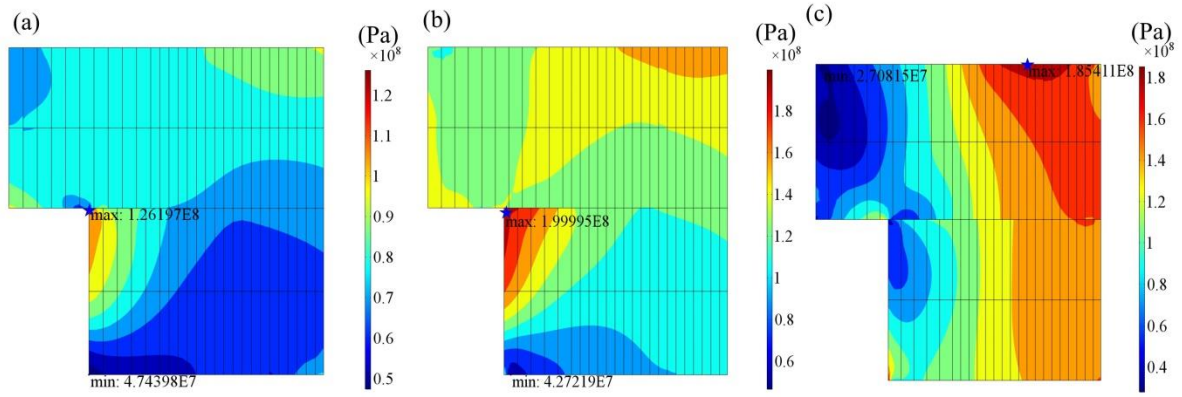

Fig. 4. Von Mises stress distribution in the coils at different steps: (a) Key insertion: the peak stress is 126 MPa and located at the corner of the center pole. (b) Cool down: the peak stress is 200 MPa and located at the corner of the center pole. (c) Excitation at 105% of the nominal current: the peak stress is 185 MPa and occurs in the upper low field region of the coil.

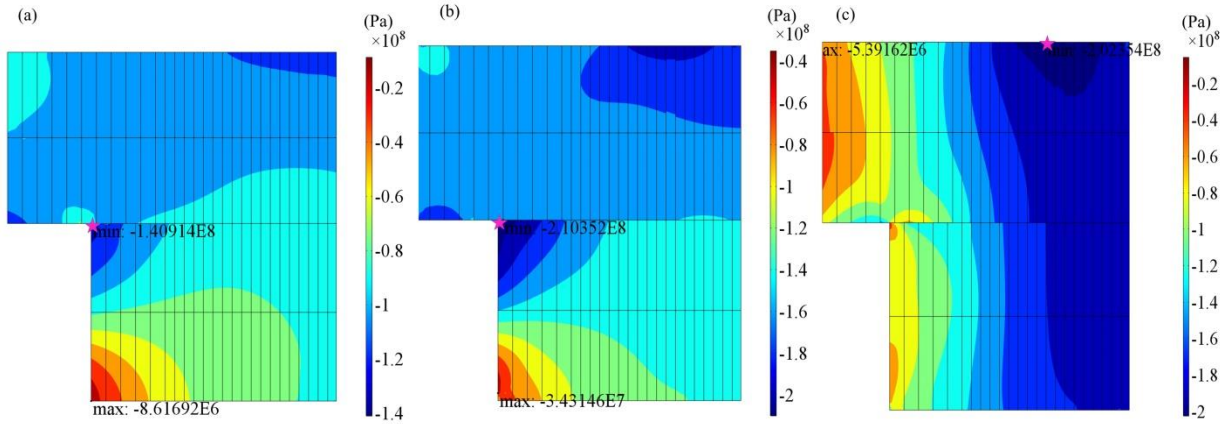

Fig. 5.Horizontal stress distribution in the coils at different step: (a) Key insertion: the peak stress is 141 MPa and located at the corner of the center pole. (b) Cool down: the peak stress is 210 MPa and located at the corner of the center pole. (c) Excitation at 105% of the nominal current: the peak stress is 202 MPa and moved in the low field region of the coil.

V. STRESS DISTRIBUTION DURING A QUENCH

In this paper, the protection system (heaters or/and CLIQ) is assumed to quench the coils totally 40 ms after an initial quench occurring spontaneously at 105% of nominal current. This 40 ms delay represents the time consumed in the quench detection and protection activation process and is based on LHC operation experience and expected quench heater performance [12]. During this 40 ms the magnet current is constant. After the 40 ms, the current starts to decay based on the magnet's resistance development and inductance. A schematic of the current decay during the quench process is shown in Fig. 6. The temperature distributions in the coils after the current decay are shown in Fig. 7. Two different cases are simulated. Case (a), the quench protection system is activated when a natural quench has not occurred which means that all the turns are still superconducting from t=0 ms to t=40 ms. Case (b), the simulation includes a hot spot turn (a turn with a natural quench) at the low field cable with the lowest temperature margin. The only difference between the hot spot turn and other turns is that during the 40 ms protection delay, heat is generated in the hot spot turn whereas other turns remain at operation temperature. Fig. 8. displays the magnet current decay and hotspot temperature development during a quench. The temperature of the hot spot reaches 356 K at the end of the quench when the hotspot is considered (case (b)). There is no heat transfer between the coils and the other components in our model.

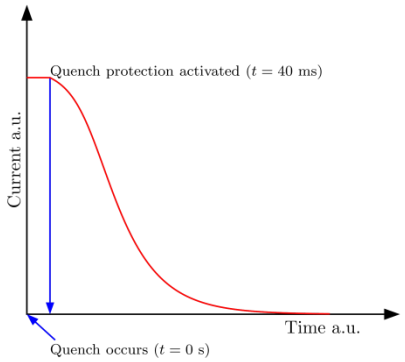

Fig. 6. A schematic of the simulated quench process.

The maximum von Mises stresses in the both situations are shown in Fig. 9. The peak von Mises stress in the coils occurs at the end of the quench and is 216 MPa when there is no natural quench. In the initial stage of the quench, the peak stress increases. Then, the current changes slightly and the temperature increases rapidly as shown in Fig. 8. After 70 ms, the peak stress decreases slightly while the current decreases rapidly. After 140 ms, the current continues to decrease while the stress in the coils increases again. After 400 ms, the current and temperature do not vary notably anymore and the maximum von Mises stress levels off. The residual stress from pre-load and the thermal stress has led to a new the stress distribution in the coils. The distribution behaviours, in terms of peak stress, are similar in both cases. The Nb_3Sn cables suffer from irreversible critical current degradation when they are directed to transverse pressure 200 MPa [20]. Thus, this state-of-the-art design, or its analysis, requires further investigation to guarantee that the magnet can survive quenches safely.

Fig. 10 and Fig. 11 show the von Mises stress distribution in the coils during the quench. The peak stress occurs in the low field region in the upper coil before 200 ms. After that, the location of the maximum von Mises stress changes to the corner of the pole. The peak stress occurs at the corner of the pole after the quench and the stress distribution behaviour is similar to the cool down process. In terms of peak stress, the distributions are similar in both cases. There is no stress accumulation occurring between the cables having the large temperature differences, e.g. the hot spot cable and its adjacent ones. This analysis suggests that it is enough to consider the stress distribution after the current has decayed. However, if the current decay and temperature evolution vary from the now considered case, one must confirm this observation.

In the previous section the peak stress was considered as the criterion for determining if a quench is a safe event. However, the strain rate may influence the validity of the plane stress assumption (static model) used in the

modelling as well as on the material properties [21]. The strain at the corner of the center pole as a function of time is shown in Fig. 12. The horizontal strain changes from 0.005 to 0.0081 and vertical strain changes from 0.0016 to 0.0056 in about 300 ms resulting in maximum strain rate on the order of 0.01 1/s. It is worth noticing that the cool down phase for a magnet lasts hours and the powering phase takes several minutes. Therefore, the dynamic loading response in case of a quench requires further analysis.

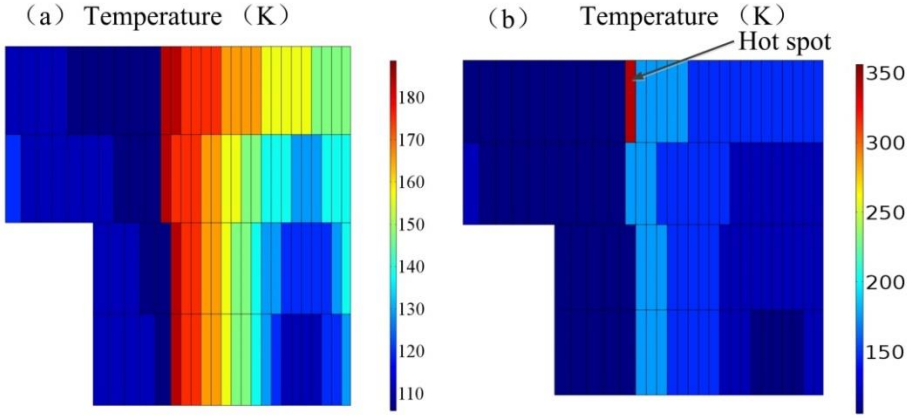

Fig. 7. The temperature distribution after the quench (a) and (b) with the hot spot turn.

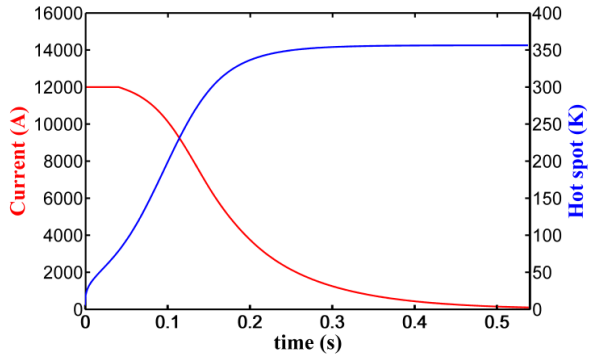

Fig. 8. The magnet current decay and hotspot temperature development

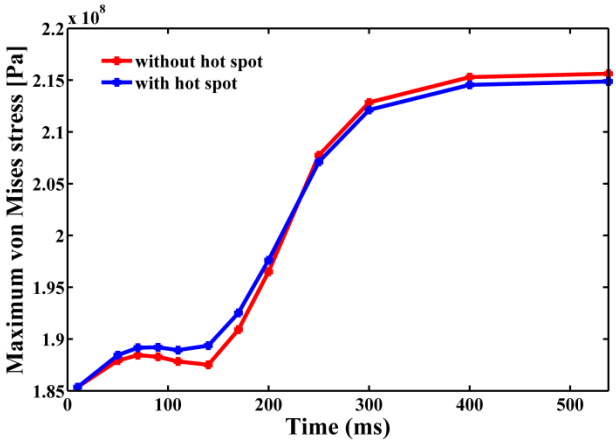

Fig. 9. The maximum von Mises stress during the quench.

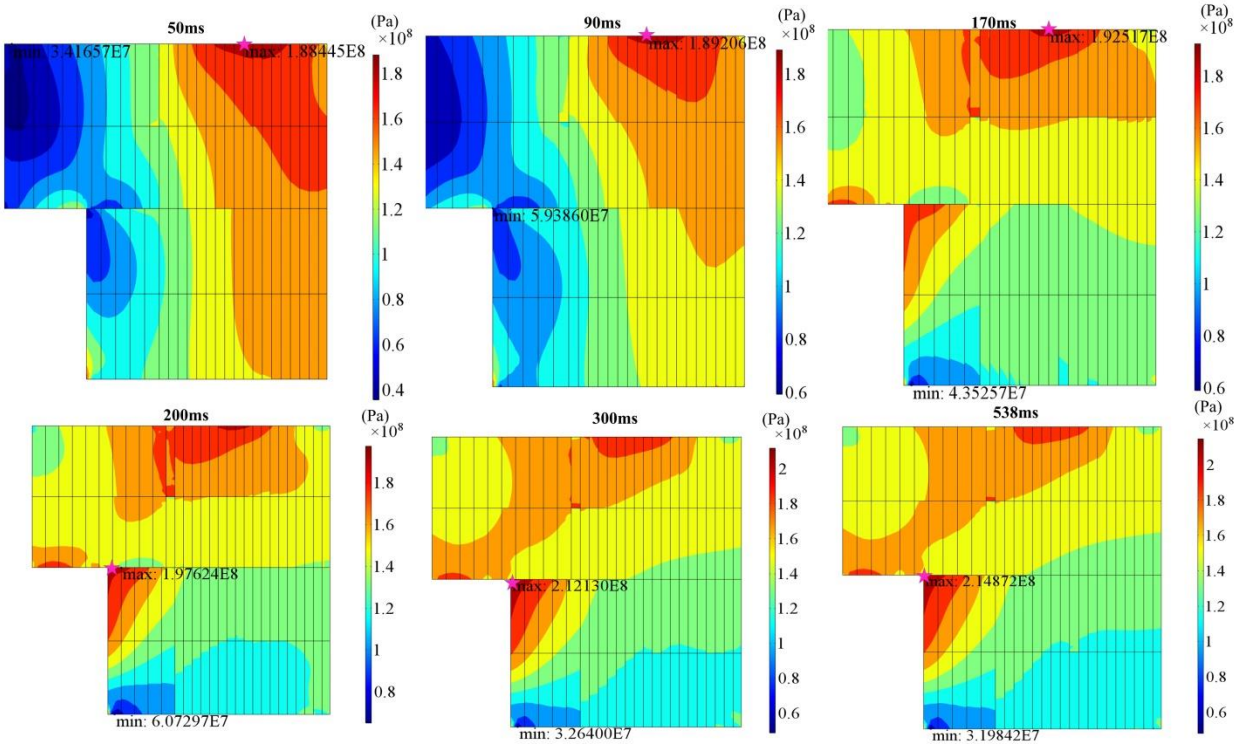

Fig 10. The von Mises stress distribution during a quench when the hot spot is not considered.

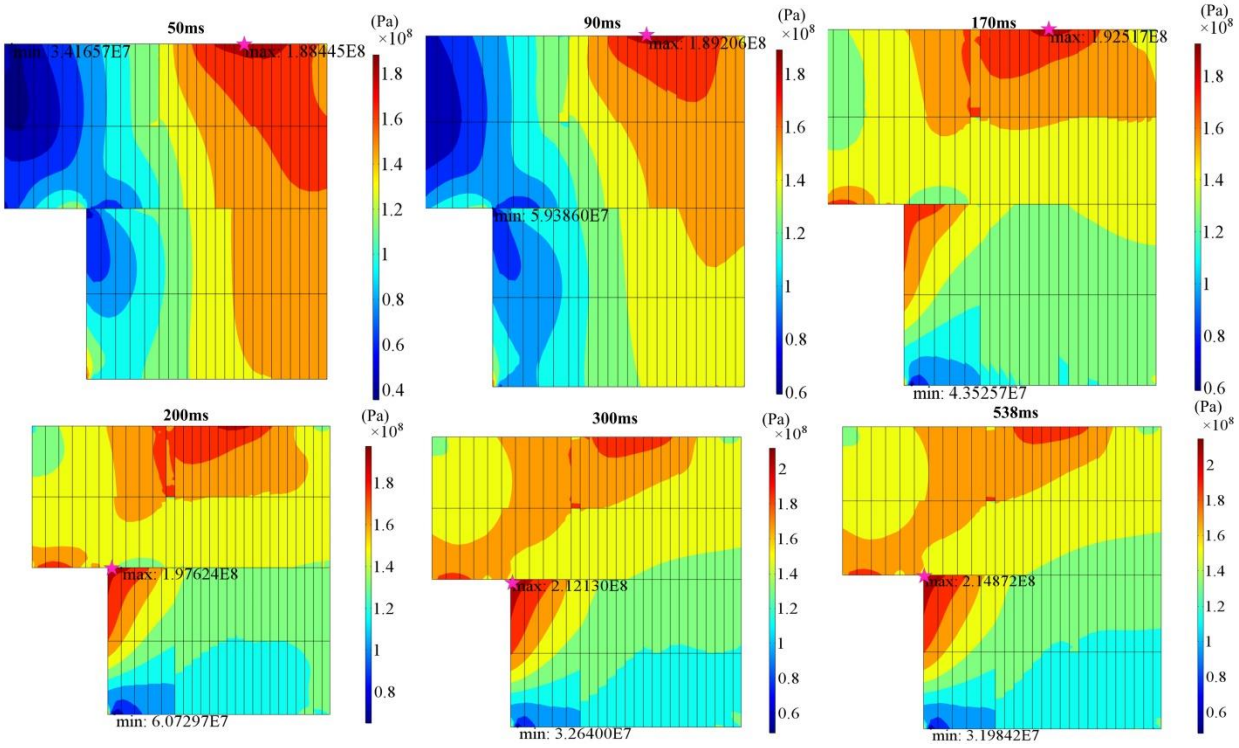

Fig 11. The von Mises stress distribution during a quench when the hot spot is considered.

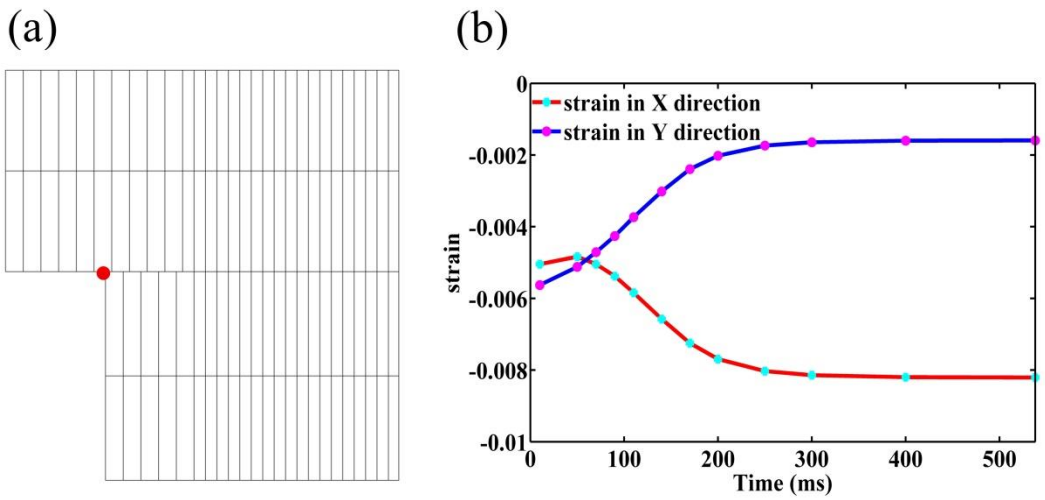

Fig. 12. The strain as a function of time (b) in presented location (a).

VI. CONCLUSIONS

The mechanical behavior of the 16 T state-of-the-art block-coil dipole magnet design for FCC during a quench has been presented. The influence of pre-load, cool down, magnet excitation, temperature evolution and current decay during the quench were considered. The evolution of the maximum von Mises stress during the quench was not monotonous in the studied cases. A local minimum was observed around 170 ms. The peak stress reached 215 MPa when the maximum hot spot temperature was 356 K. In the two simulated cases, where one ignores the hot spot turn and other considers it, the peak von Mises stress was similar as a function of time during the quench. Our analysis suggests that it is enough to consider the stress distribution after the current decay to find the worst case scenario. However, this conclusion cannot be taken for granted for any magnet since we considered only one case, employing 2-D model with homogenized cable internal structure. The dynamic loading response during a quench requires further analysis.

VII. ACKNOWLEDGEMENT

This work was supported by the academy of Finland projects (287027 and 295185), European Union's Horizon 2020 research and innovation programme under grant 654305, EuroCirCol project, the China Scholarship Council, the National Natural Science Foundation of China (11572143, 11372120 and 11421062).

REFERENCE

[1] Future Circular study website. https://fcc.web.cern.ch/, 18, Feb. 2017.

[2] Horizon 2020 EuroCirCol Consortium Agreement, number 654305.

[3] Future Circular study website. https://fcc.web.cern.ch/Pages/Magnets.aspx , 22 Feb. 2017.

[4] D. Tommasini et al., "The 16 T dipole development program for FCC". *IEEE Trans. Appl. Supercond.*, vol. 27, no. 4, Jun. 2017, Art. ID 4000405.

[5] F. Toral et al., "EuroCirCol 16T common-coil dipole option for the FCC". *IEEE Trans. Appl. Supercond.*, vol. 27, no. 4, Jun. 2017, Art. ID 4001105.

[6] C. Lorin et al., "EuroCirCol 16 T block-coils dipole option for the future circular collider." *IEEE Trans. Appl. Supercond.*, vol. 27, no. 4, Jun. 2017, Art. ID 4001405.

[7] S. Caspi et al., "Design of a Canted-Cosine-Theta Superconducting Dipole Magnet for Future Colliders," in IEEE Transactions on Applied Superconductivity, vol. 27, no. 4, pp. 1-5, June 2017. Art. ID 4001505.

[8] M. Sorbi et al., "The EuroCirCol 16T Cosine–Theta Dipole Option for the FCC," *IEEE Trans. Appl. Supercond.*, vol. 27, no. 4, pp. 1-5, Jun. 2017. Art. ID 4001205.

[9]F.L. Goodrich et al., "Method for determining the irreversible strain limit of Nb3Sn wires". Supercond. Sci. Technol., vol. 24, p. 075022, 2011.

[10] E. Todesco., "Quench limits in the next generation of magnets," CERN, Geneva, Switzerland, CERN Yellow Rep. CERN-2013-006, Jan. 2014, pp. 10–16.

[11] E. Ravaioli et al., "Quench Protection of a 16-T Block-Coil Dipole Magnet for a 100-TeV Hadron Collider Using CLIQ." *IEEE Trans. Appl. Supercond.*, vol. 26, no. 4, Jun. 2016. Art. ID 4002307.

[12] T. Salmi et al., "Quench protection analysis integrated in the design of dipoles for the Future Circular Collider," in Phys. Rev. ST Accel. Beams, accepted 2017.

[13] COMSOL. Inc. https://www.comsol.com, 22 Feb, 2017.

[14] S. Caspi., "The use of pressurized bladders for stress control of superconducting magnets," *IEEE Trans. Appl. Supercond.*, vol. 16, pt. 2, pp. 358–361, Jun. 2006.

[15] BERKELEY LAB. http://newscenter.lbl.gov/2011/12/13/clyde-taylor/, 23 Feb. 2017.

[16] K. zhang et al., "2-D mechanical design study of a 20-T two-in-one common-coil dipole magnet for high-energy accelerators." *IEEE Trans. Appl. Supercond.* vol. 26, no. 4, Jun. 2016. Art. ID 4003705.

[17] C. Lorin, M. Durante, M. Segreti, "16 T Nb_3Sn block dipole EuroCirCol", this conference.

[18] S. Caspi et al., "Fabrication and Test of TQS01—A 90 mm Nb3Sn Quadrupole Magnet for LARP," *IEEE Trans. Appl. Supercond.*, vol. 17, no. 2, pp. 1122-1125, Jun. 2007.

doi: 10.1109/TASC.2007.899244.

[19] M. Juchno et al., "Support Structure Design of the Nb_3Sn Quadrupole for the High Luminosity LHC," *IEEE Trans. Appl. Supercond.*, vol. 25, no. 3, pp. 1-4, Jun. 2015.

[20] D. R. Dietderich et al., "Nb3Sn research and development in the USA—Wires and cables," *Cryogenics*, vol. 48, no. 7/8, pp. 331–340, Jul./Aug. 2008.

[21] A. S. Khan et al., "Quasi-static and dynamic loading responses and constitutive modeling of titanium alloys," Int. J. Plast., vol. 20, pp. 2233-2248, July. 2004.